Solar Energy Materials & Solar Cells 214 (2020) 110585

Contents lists available at ScienceDirect

Solar Energy Materials and Solar Cells

journal homepage: http://www.elsevier.com/locate/solmat

Fully screen-printed bifacial large area 22.6% N-type Si solar cell with lightly doped ion-implanted boron emitter and tunnel oxide passivated rear contact

Ying-Yuan Huang, Young-Woo Ok *, Keeya Madani, Wookjin Choi, Ajay D. Upadhyaya, Vijaykumar D. Upadhyaya, Ajeet Rohatgi

Georgia Institute of Technology, 777 Atlantic Drive, Atlanta, GA, 30332, United States

ARTICLE INFO

Keywords:
TOPCon
Passivating contacts
Poly-silicon
Screen printing
Implanted B emitter
Large area
Bifacial cell

ABSTRACT

We report on the fabrication of fully screen-printed bifacial large area (239 cm^2) high-efficiency n-type Si solar cells with ion-implanted homogeneous boron emitter on the front side and carrier-selective tunnel oxide passivated contact (TOPCon) on the rear. Our phosphorus-doped poly-Si/SiO_x passivated contact with SiN_x capping layer gave excellent surface passivation with a very low recombination current density (J_{0_TOPCon}) of ~1 fA/cm^2 after a simulated firing treatment at ~770 °C without metallization. After screen-printed and fire-through metallization on n-TOPCon with ~13% metal coverage, metallized J_{0_TOPCon} value increased to only ~5 fA/cm^2. In addition, homogenous boron implanted emitter (~180 Ω/) passivated with ALD Al_2O_3 layer capped with PECVD SiN_x/SiO_x double-layer antireflection (DLAR) coating gave excellent passivation with emitter recombination current density of ~12 fA/cm^2 prior to metallization. The industrial screen-printed, fire-through contacts with floating busbars on this boron emitter gave metallized emitter recombination current density of ~31 fA/cm^2. This resulted in a low-cost industrial screen-printed n-type bifacial Si solar cell with 22.6% efficiency and 702 mV open-circuit voltage (V_{oc}).

1. Introduction

SiO_x/poly-Si (polycrystalline silicon) carrier-selective passivating contacts, such as tunnel oxide passivated contact (TOPCon), have become an active research area for next-generation industrial silicon solar cells due to the excellent surface passivation, elimination of diffusion into the bulk, no direct metal contact to absorber material, and ability to withstand high temperature [1–5]. An n-type TOPCon (n-TOPCon) is composed of a very thin tunnel oxide (SiO_x) capped with phosphorus doped n^+ poly-Si. Several investigators have reported very low recombination current density (J_0) (<10 fA/cm^2) [6–10] for n-TOPCon structure with ≤1.5 nm SiO_x capped with n^+ doped poly-Si. As a result, very high efficiency (>25.7%) small area R&D cells have been reported but with full area evaporated Ag on n-TOPCon on the rear [11]. However, to adapt TOPCon technology for industrial production of large-area Si solar cells, several challenges need to be overcome, including screen-printing induced shunting and degradation of J_0 of n-TOPCon with thin poly-Si [12], parasitic absorption in the doped poly-Si [13,14], single-side deposition of poly-Si [15], and throughput [16]. The poly-Si thickness needs to be adequate to prevent the penetration of the fire-through metal paste into the thin oxide and oxide/Si interface. This is essential for achieving the lowest metallized J_0 for the TOPCon layer. Recently few investigators have reported low metallized J_0 for fire through screen-printed contacts to n-TOPCon using thicker poly-Si layers, which resulted in cell efficiencies of 21–23.5% [8,12, 17–22]. However, thicker poly-Si increases parasitic absorption which decreases short circuit current [13,14]. Recently, Nandakumar et al. reported on reduced parasitic absorption when thick poly-Si layers are partially oxidized during deposition without hurting passivation and contact properties [23], resulting in a ~23.05% large area, screen-printed n-TOPCon bifacial cell. In addition, they used a plasma-enhanced chemical vapor deposition (PECVD) tool to grow in-situ tunnel oxide and thick n^+ poly-Si in a single step on one side only with very high deposition rate, which brings the TOPCon technology much closer to mass production. In spite of these encouraging results, there is limited quantitative understanding of J_0 contribution from each

* Corresponding author.
E-mail address: yok6@mail.gatech.edu (Y.-W. Ok).

https://doi.org/10.1016/j.solmat.2020.110585
Received 20 December 2019; Received in revised form 28 April 2020; Accepted 28 April 2020
Available online 16 May 2020

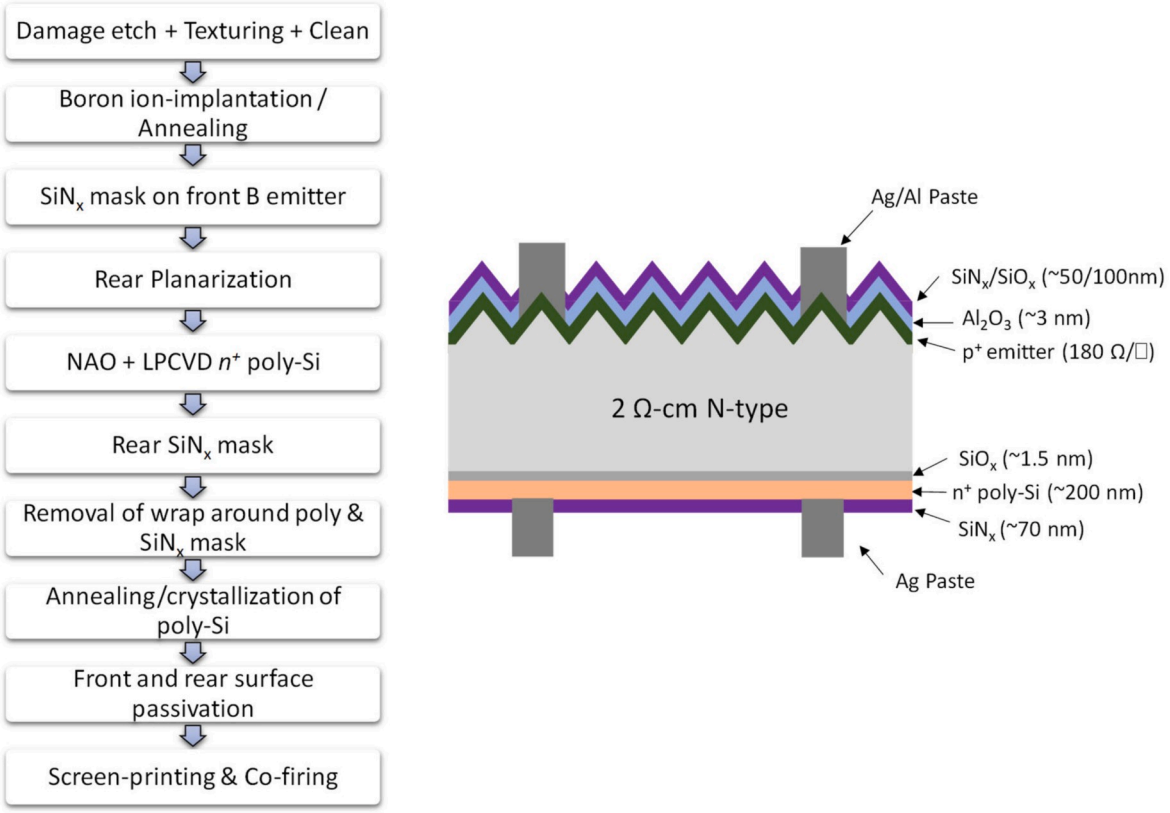

Fig. 1. Process sequence and structure of the screen-printed bifacial n-type Si solar cell with front implanted boron emitter and rear tunnel oxide passivated contact.

layer, bulk lifetime, and contact parameters of fully screen-printed high-efficiency TOPCon cells. This paper reports on the fabrication as well as detailed analysis of such high efficiency commercial size bifacial cells with screen-printed metallization on both sides.

In this paper, industrial size high efficiency fully screen-printed bifacial n-type solar cells were fabricated with ion-implanted homogeneous front boron (B) emitter and rear n-TOPCon. A co-firing process was used to make screen-printed contacts to lightly doped B emitter and n-TOPCon simultaneously. The benefit of floating busbars was also quantitatively examined for the lightly doped implanted homogeneous B emitter by modeling, fabrication, and characterization of cells with five floating as well as fire-through busbars.

2. Experimental

Fig. 1 shows the process flow and structure of the large-area (239 cm^2) n-type bifacial cells fabricated with an implanted B emitter on front and low pressure chemical vapor deposition (LPCVD) grown n-TOPCon on rear side of 180 μm thick 2 Ω-cm n-type Cz wafers. Since LPCVD grows poly-Si on both sides of the wafer, we implemented a masking process to etch poly-Si from front side. After standard saw damage etching, texturing and cleaning, the wafers received B ion implantation on the front side with a dose of 1.2e15/cm^2 at 10 KeV ion energy followed by an annealing and oxidation process at high temperature (~1050 °C), which resulted in sheet resistance of 180 Ω/. After the removal of oxide thermally grown during the implant anneal, a PECVD SiN_x was deposited on the front side as a mask to protect the emitter during back planarization and front poly-Si etching. A heated KOH treatment was used to planarize the back. After an acid clean and HF dip, a ~15 Å tunnel oxide layer was grown by nitric acid oxidation (NAO) at 100 °C for ~10 min [24], followed by 200 nm LPCVD n^+ poly-Si deposition at 580 °C with in-situ phosphorus doping. Next, a PECVD SiN_x masking layer was deposited on the back poly-Si, and then the front poly-Si was removed by wet etching in KOH solution. After that, both front and back SiN_x masks were removed by HF treatment. The samples were then annealed at 855 °C for poly-Si crystallization and dopant activation. The B emitter was then passivated by atomic layer deposition (ALD) of Al_2O_3 and PECVD SiN_x/SiO_x stack while the back poly-Si was capped with ~700 Å thick PECVD SiN_x layer. For cells with non-floating busbars, 40 μm wide 104 grid lines in combination with 600 μm wide 5

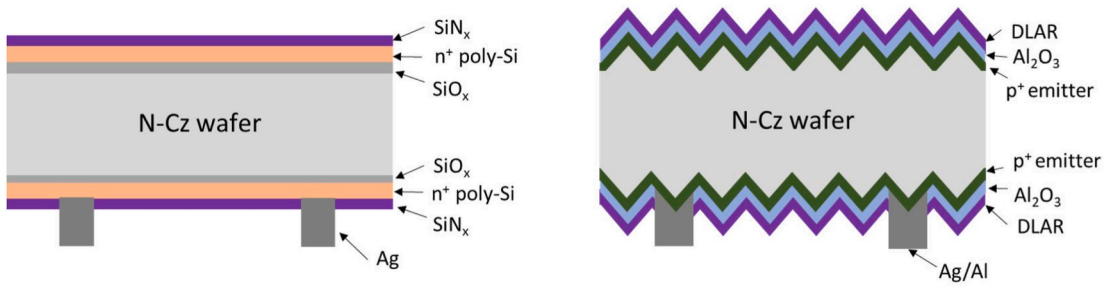

Fig. 2. Schematic of n-TOPCon and implanted boron emitter test structures to investigate the impact of screen-printed metallization on J_0.

Table 1
Light I–V results of best screen-printed, large-area n-TOPCon bifacial cells with non-floating busbars (nFB) and floating busbars (FB).

Busbar	V_{OC} [mV]	J_{SC} [mA/cm^2]	FF [%]	η [%]	n-factor	Rs [Ω-cm^2]	Rsh[Ω-cm^2]	pFF[%]
nFB	688	40.1	80.0	22.1	1.17	0.41	5270	82.3
FB	702	40.3	79.7	22.6	1.12	0.59	12800	82.7

busbars were screen-printed on the B emitter using a fire through Ag/Al paste and single print. The screen grid opening was 35 μm, resulting in fired grid linewidth of 40 μm. Front side metallization with floating busbars (FB) was done using dual-print, where the grid fingers were screen-printed first using the fire-through Ag/Al paste first and then a fritless non-fire-through Ag paste was used to print the busbars. Next, 60 μm wide 300 grid lines in combination with 600 μm wide 5 busbars were screen-printed on the rear n-TOPCon using fire-through Ag paste and single print. Finally, all samples were co-fired in an industrial-style belt furnace with peak firing temperature of 770 °C. The two SiN_x masking steps employed in our cell fabrication process can be eliminated by the single side etching tool used in industrial setting.

During the cell fabrication, symmetrical test structures of n-TOPCon and implanted B emitter were prepared to quantify their passivation properties and the impact of screen-printed metallization (Fig. 2). The symmetric p^+np^+ test structures were passivated with thin Al_2O_3 capped with PECVD SiN_x/SiO_x on textured Si wafers to determine the J_0 of the implanted B emitter using the photoconductance decay (PCD) measurement technique proposed by Kane and Swanson [25]. Similarly, symmetric LPCVD grown n-TOPCon structures were prepared on planar Si wafers capped with SiN_x for the J_0 measurements. In order to quantify the effect of screen-printed fire-through metallization on recombination current density of our implanted B emitter (J_{0e}) and rear n-TOPCon (J_{0_TOPCon}), gridlines with different metal coverage were screen-printed only on one side of the symmetric structures. After the simulated contact firing, the excess printed metal was etched away in $HCl:H_2O_2:H_2O$ = 1:1:1 solution, leaving only the embedded metal contact on the surface for the metallized J_0 measurements.

3. Results and discussion

Table 1 shows the cell parameters from light I–V measurements when the cell is illuminated from the front side. Cells were measured in-house using the Fraunhofer ISE certificated reference cell. The fire-through busbar cells showed best cell efficiency of 22.1% with V_{oc} of 688 mV, J_{sc} of 40.1 mA/cm^2, and *FF* of 80.0%. However, the best cell with floating busbars showed ~14 mV higher V_{oc}, resulting in a V_{oc} of 702 mV and efficiency of ~22.6%. The efficiency range was 22.0–22.1% for non-floating busbar, and 22.4–22.6% for floating busbar cells. Both cells showed high J_{SC} (>40 mA/cm^2) due to high EQE, reduced shading from narrow lines, and SiO_2/SiN_x two-layer AR coating on front.

For the quantitative study of the effect of screen-printed fire-through metallization on recombination current density of our implanted B emitter and rear n-TOPCon, the above test structures with different metal fraction on one side (Fig. 2) were measured by the PCD tester with the light flashing on the no-metal side to avoid any shading effect. In addition, specific contact resistance was measured using TLM pattern on the same samples, resulting in 2 and 4 mΩ-cm^2 values for the n-TOPCon and B emitter, respectively, supporting the excellent co-firing process for front and back metallization. Fig. 3(a) shows the measured total J_0 from the n-TOPCon test structures as a function of metal fraction on one side. The total measured J_0 of the test structures with different metal fractions (f) on one side can be expressed as

$$\begin{aligned} Total\ J_0 &= J_{0\_TOPCon(no\ metal)} + J_{0\_TOPCon(with\ metal\ fraction\ f)} \\ &= J_{0\_TOPCon,pass} + \left[J_{0\_TOPCon,pass} \times (1-f) + J_{0\_TOPCon,metal} \times f\right] \\ &= \left(J_{0\_TOPCon,metal} - J_{0\_TOPCon,pass}\right) \times f + 2\,J_{0\_TOPCon,pass} \end{aligned}$$

where $J_{0\_TOPCon,\ pass}$ and $J_{0\_TOPCon,\ metal}$ are the full area J_0 values for the un-metallized and metallized n-TOPCon. Fig. 3 (a) shows that without any metal, total J_0 (=2 × $J_{0\_TOPCon,\ pass}$) of ~2 fA/cm^2 was achieved, which corresponds to a $J_{0\_TOPCon,\ pass}$ of ~1 fA/cm^2, indicating excellent passivation quality of our SiN_x capped LPCVD grown unmetallized n-TOPCon after simulated contact firing. However, total J_{0_TOPCon} did show a slight increase with increased metal fraction (Fig. 3 (a)). From the intercept and slope of the linear fit to the experimental data in Fig. 3 (a) (y = 29.3 x + 2.1), we obtained a $J_{0\_TOPCon,\ metal}$ ~30 fA/cm^2 and $J_{0\_TOPCon,\ pass}$ ~ 1.05 fA/cm^2 for the metallized and unmetallized n-TOPCon regions. This corresponds to a metallized J_{0_TOPCon} of 5 fA/cm^2 (= 30 × 13.5% + 1 × 86.5%) for 13.5% metal coverage on the back, resulting from 60 μm wide 300 grid lines and 600 μm wide 5 busbars in this study. Identical study was conducted on B emitter test structures from which full area $J_{0e,metal}$ = ~706 fA/cm^2 and $J_{0e,pass}$ = ~12 fA/cm^2 were obtained for our 180 Ω/□ implanted B emitter, as shown in Fig. 4 (b). This corresponds to a metallized J_{0e} of 31 fA/cm^2 (= 706 × 2.7% + 12 × 97.3%) for 2.7% metal/Si contact fraction for floating busbars and

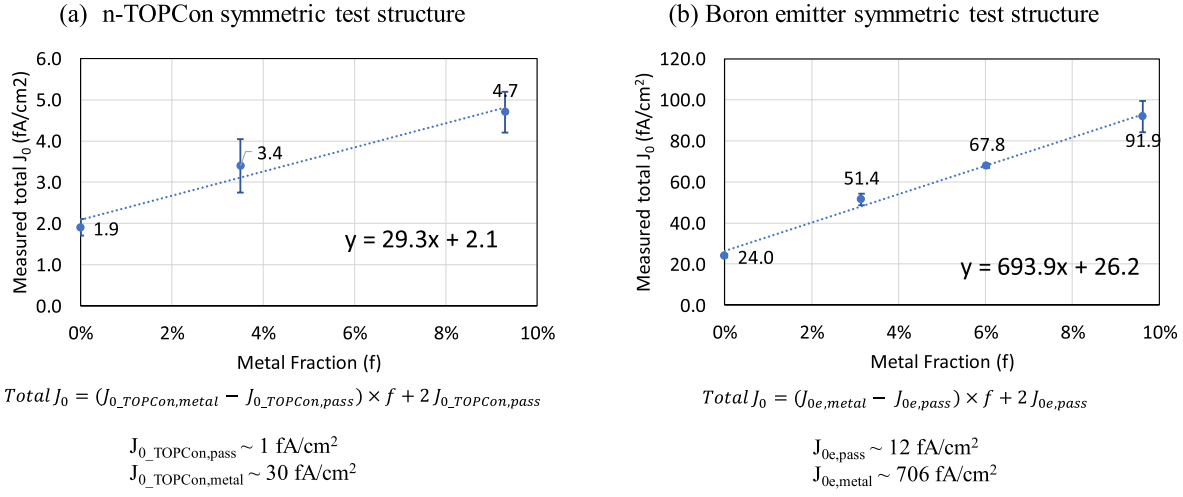

Fig. 3. Measured recombination current density (J_0) from (a) n-TOPCon and (b) boron implanted emitter as a function of metal fraction on one side.

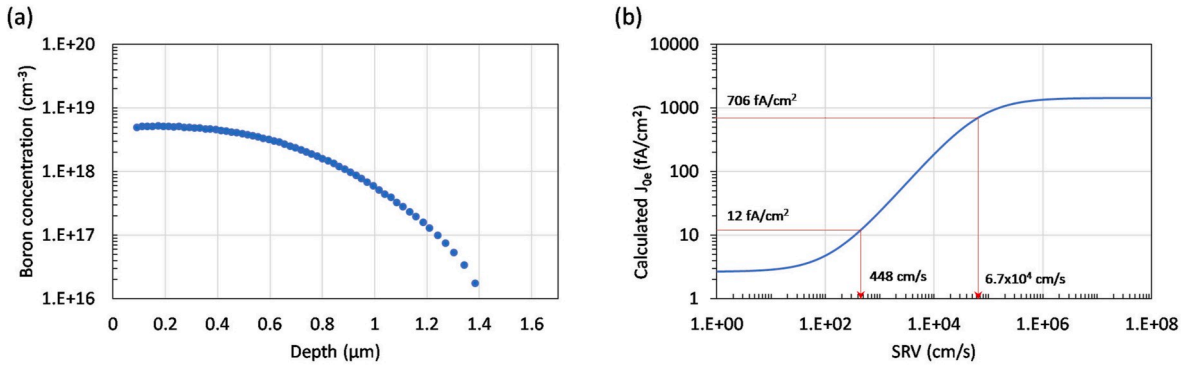

Fig. 4. Measured implanted B profile (a) and calculated J_{0e} as functions of surface recombination velocity (b).

44 fA/cm^2 (= 706 × 4.6% + 12 × 95.4%) for non-floating busbars (4.6% metal fraction). From the measured cell J_{sc} and V_{oc}, a total J_0 of 58 fA/cm^2 was obtained ($V_{OC} = \frac{kT}{q}\ln\left(\frac{J_{SC}}{J_0}\right)$). Finally, J_{0_bulk} was calculated to be 22 fA/cm^2 by subtracting the metallized J_{0e} (31 fA/cm^2) and metallized J_{0_TOPCon} (5 fA/cm^2) from the total J_0 (58 fA/cm^2). This cell analysis reveals that the V_{OC} of 22.6% cell is limited by the recombination in the bulk and emitter because the metallized J_0 of our TOPCon layer is very small (~5 fA/cm^2). Table 2 summarizes all the J_0 components in our 22.6% efficient finished cell.

Additional characterization and modeling was performed to improve the fundamental understanding of our 22.6% cell. We used the Sentaurus 2D simulator for modeling which requires surface recombination velocities on the B emitter and n-TOPCon regions rather than J_0 values. Fig. 4 (a) shows the measured profile of our implanted B emitter with ~5 × 10^{18}/cm^3 surface concentration and junction depth of ~1.4 μm. Fig. 4 (b) shows the calculated J_{0e} as function of surface recombination velocity for this B emitter profile, obtained from Sentaurus simulation [26,27]. From Fig. 4 (b), a surface recombination velocity value of 448 cm/s was obtained for the unmetallized passivated emitter region, using the measured J_{0e} = 12 fA/cm^2 (Fig. 3(b)). Similarly, SRV of ~6.7 × 10^4 cm/s was extracted (Fig. 4 (b)) for the metallized emitter region from the measured $J_{0e,metal}$ of 706 fA/cm^2 (Fig. 3(b)). Since the exact tunneling mechanism and tunneling parameters were not fully known for our TOPCon, we measured phosphorus in-diffusion profile in Si bulk by electrochemical capacitance-voltage (ECV) technique and replaced the n-TOPCon region by this profile with an effective surface recombination velocity that produce a J_0 = 5 fA/cm^2, which is equal to the measured metallized J_0 value of the TOPCon. This profile is formed during the 855 °C n-TOPCon anneal, and has a junction depth of 0.06 μm and a surface concentration of 4.7 × 10^{18} cm^{-3} (Fig. 5 (a)). Sentaurus model was used to generate the J_0 vs S curve for this profile (Fig. 5(b)) from which an effective hole SRV of 328 cm/s was extracted at the tunnel oxide/Si interface using the metallized J_{0_TOPCon} value of 5 fA/cm^2. This approach is similar to the one used by Chen et al. [28]. Finally, a complete Sentaurus 2D model was built to match the 22.6% efficient screen-printed TOPCon solar cell using all the measured material and device parameters (contact area, shading area and contact resistance) and the extracted recombination velocities at the passivated and metallized emitter regions and the tunnel oxide/Si interface (Table 4 column 1). The modeled cell parameters matched very well with the measured cell light IV (LIV)

Table 2
Summary of recombination current density for each region of our 22.6% n-TOPCon cell.

Cell regions	Full area (100%) J_0 (fA/cm^2)	Area fraction (%)	Area-weighted J_0 (fA/cm^2)
Passivated boron emitter	12	97.3%	11.7
Metallized boron emitter	706	2.7%	19.1
Bulk	22	100%	21.8
Rear passivated TOPCon	1	86.5%	0.9
Rear metallized TOPCon	30	13.5%	4.0
Full Cell			57.5

Table 3
Comparison of measured and modeled screen-printed TOPCon solar cell parameters.

	V_{OC} (mV)	J_{SC} (mA/cm^2)	FF (%)	Eff (%)
Experiment	702	40.3	79.7	22.6
Model	701	40.3	79.6	22.5

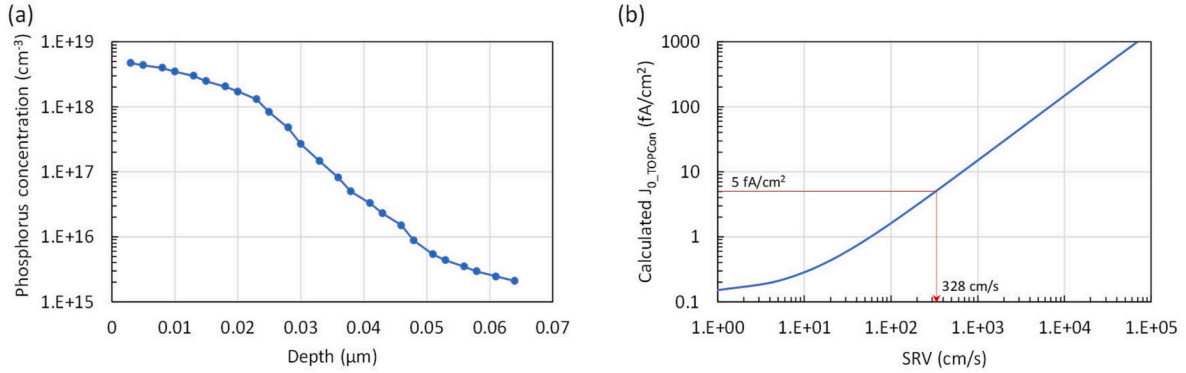

Fig. 5. Measured phosphorus in-diffusion profile in bulk Si (a) and calculated J_{0_TOPCon} as functions of effective hole surface recombination velocity (b).

Table 4
Sentaurus 2D modeling of the 22.6% TOPCon cell and a roadmap to ~ 24% efficiency.

Parameters	22.6% floating busbar TOPCon cell	30 Ω/□ selective emitter	3 ms bulk lifetime	Multiwire contact
Voc [mV]	701	704	709	710
Jsc [mA/cm^2]	40.3	40.3	40.3	40.7
FF [%]	79.6	80.1	81.8	82.8
Efficiency [%]	22.5	22.7	23.4	23.9
Front finger width W_f (μm)	40	40	40	40
Front shading coverage	4.59%	4.59%	4.59%	3.56%
Busbar number/ width (μm)	5/600	5/600	5/600	14/100
Wafer thickness (μm)	180	180	180	180
Field emitter profile	Measured	Measured	Measured	Measured
Field emitter sheet resistance (Ω/□)	~180	~180	~180	~180
Front contact resistance (mΩ-cm^2)	4	1	1	1
Selective emitter profile	N/A	Measured	Measured	Measured
Selective emitter sheet resistance (Ω/□)	N/A	~30	~30	~30
Selective emitter surface concentration (cm^{-3})	N/A	$\sim 3 \times 10^{19}$	$\sim 3 \times 10^{19}$	$\sim 3 \times 10^{19}$
Selective emitter junction depth (μm)	N/A	1.9	1.9	1.9
Selective emitter junction width (μm)	N/A	100	100	100
Substrate resistivity (Ω-cm)	2	2	2	2
Substrate doping (cm^{-3})	2.38×10^{15}	2.38×10^{15}	2.38×10^{15}	2.38×10^{15}
Front passivated FSRV (cm/s)	448	448	448	448
Wing FSRV (cm/s)	N/A	721	721	721
Front contact FSRV (cm/s)	6.7×10^4	10^7	10^7	10^7
Lifetime (ms)	1	1	3	3
Back contact resistance (mΩ-cm^2)	2	2	2	2
Back contact hole SRV at n + Si/ tunnel oxide interface (cm/s)	328	328	328	328

data, as shown in Table 3. In order to establish directions for further efficiency improvement, we extended the 2D Sentaurus modeling. Table 4 shows that a combination of selective emitter (30/180 Ω/□), increased bulk lifetime from 1 to 3 ms, and 100 μm wide 14 floating busbars for multiwire application can raise the cell efficiency to ~ 24%.

4. Conclusions

A fully screen-printed large area ~22.6% efficient bifacial n-type Si solar cell was fabricated with implanted lightly doped homogeneous B emitter (180 Ω/□) on the front and n-TOPCon on the back of a 2 Ω-cm n-type Cz Si. SiN_x capped LPCVD grown 200 nm n^+ poly-Si on ~15 Å tunnel oxide produced unmetallized J_0 value of ~1 fA/cm^2 and metallized J_0 of ~5 fA/cm^2 with 13.5% metal coverage. Floating busbars on the front emitter gave ~14 mV increase in V_{OC} with ~0.5% efficiency enhancement due to reduced front metal/Si contact area on the lightly doped B emitter. Detailed analysis was performed to determine the J_0 component and interface recombination velocity of each region. Results indicated that the metallized J_0 of the lightly doped B emitter (J_{0e} = ~31 fA/cm^2) and ~1 ms bulk lifetime wafer (J_{0_bulk} = 22 fA/cm^2) limited the voltage to 702 mV and cell efficiency to 22.6%. Model calculations also showed that a combination of B selective emitter, improved bulk lifetime and multiwire contacts on the front can raise the cell efficiency to ~24%.

Declaration of competing interest

The authors declare that they have no known competing financial interests or personal relationships that could have appeared to influence the work reported in this paper.

CRediT authorship contribution statement

Ying-Yuan Huang: Conceptualization, Methodology, Validation, Formal analysis, Investigation, Data curation, Writing - review & editing, Visualization. **Young-Woo Ok:** Investigation, Writing - review & editing, Visualization, Supervision. **Keeya Madani:** Investigation, Formal analysis. **Wookjin Choi:** Investigation, Formal analysis. **Ajay D. Upadhyaya:** Investigation, Formal analysis. **Vijaykumar D. Upadhyaya:** Investigation. **Ajeet Rohatgi:** Project administration, Funding acquisition, Supervision.

Acknowledgements

The authors would like to thank Tran-Vinh Nguyen and Chris (Yeyuan) Yang from the Institute for Electronics and Nanotechnology, Georgia Institute of Technology for their technical support. This material is based upon work supported by the U.S. Department of Energy's Office of Energy Efficiency and Renewable Energy (EERE) under Solar Energy Technologies Office (SETO) Agreement Number DE-EE0007554.

Appendix A. Supplementary data

Supplementary data to this article can be found online at https://doi.org/10.1016/j.solmat.2020.110585.

References

[1] F. Feldmann, M. Bivour, C. Reichel, M. Hermle, S.W. Glunz, Passivated rear contacts for high-efficiency n-type Si solar cells providing high interface passivation quality and excellent transport characteristics, Sol. Energy Mater. Sol. Cell. 120 (2014) 270–274. Part A.
[2] P. Stradins, S. Essig, W. Nemeth, B. Lee, D. Young, A. Norman, Y. Liu, J. Luo, E. Warren, A. Dameron, Passivated tunneling contacts to N-type wafer silicon and their implementation into high performance solar cells, in: Proc. 6th WCPEC, 2014. Kyoto, Japan.
[3] A. Moldovan, F. Feldmann, M. Zimmer, J. Rentsch, J. Benick, M. Hermle, Tunnel oxide passivated carrier-selective contacts based on ultra-thin SiO2 layers, Sol. Energy Mater. Sol. Cell. 142 (2015) 123–127.
[4] Y.-W. Ok, A.M. Tam, Y.-Y. Huang, V. Yelundur, A. Das, A.M. Payne, V. Chandrasekaran, A.D. Upadhyaya, A. Jain, A. Rohatgi, Screen printed, large area bifacial N-type back junction silicon solar cells with selective phosphorus front surface field and boron doped poly-Si/SiOx passivated rear emitter, Appl. Phys. Lett. 113 (2018) 263901.
[5] A. Rohatgi, B. Rounsaville, Y.-W. Ok, A.M. Tam, F. Zimbardi, A.D. Upadhyaya, Y. Tao, K. Madani, A. Richter, J. Benick, M. Hermle, Fabrication and modeling of high-efficiency front junction N-type silicon solar cells with tunnel oxide passivating back contact, IEEE Journal of Photovoltaics (2017) 1–8.
[6] R. Peibst, Y. Larionova, S. Reiter, M. Turcu, R. Brendel, D. Tetzlaff, J. Krügener, T. Wietler, U. Höhne, J.-D. Kähler, H. Mehlich, S. Frigge, Implementation of N+ and P+ POLO Junctions on Front and Rear Side of Double-Side Contacted Industrial Silicon Solar Cells, 2016.
[7] Y. Tao, V. Upadhyaya, C.-W. Chen, A. Payne, E.L. Chang, A. Upadhyaya, A. Rohatgi, Large area tunnel oxide passivated rear contact n-type Si solar cells with 21.2% efficiency. Progress in Photovoltaics: Research and Applications, 2016 n/a-n/a.
[8] M.K. Stodolny, M. Lenes, Y. Wu, G.J.M. Janssen, I.G. Romijn, J.R.M. Luchies, L. J. Geerligs, n-Type Polysilicon Passivating Contact for Industrial Bifacial N-type Solar Cells, Solar Energy Materials and Solar Cells, 2016.

[9] J. Melskens, B.W.H.v.d. Loo, B. Macco, L.E. Black, S. Smit, W.M.M. Kessels, Passivating contacts for crystalline silicon solar cells: from concepts and materials to prospects, IEEE Journal of Photovoltaics 8 (2018) 373–388.
[10] J. Schmidt, R. Peibst, R. Brendel, Surface passivation of crystalline silicon solar cells: present and future, Sol. Energy Mater. Sol. Cell. 187 (2018) 39–54.
[11] A. Richter, J. Benick, F. Feldmann, A. Fell, M. Hermle, S.W. Glunz, n-Type Si solar cells with passivating electron contact: identifying sources for efficiency limitations by wafer thickness and resistivity variation, Sol. Energy Mater. Sol. Cell. 173 (2017) 96–105.
[12] P. Padhamnath, J. Wong, B. Nagarajan, J.K. Buatis, L.M. Ortega, N. Nandakumar, A. Khanna, V. Shanmugam, S. Duttagupta, Metal contact recombination in monoPoly™ solar cells with screen-printed & fire-through contacts, Sol. Energy Mater. Sol. Cell. 192 (2019) 109–116.
[13] F. Feldmann, C. Reichel, R. Müller, M. Hermle, The application of poly-Si/SiOx contacts as passivated top/rear contacts in Si solar cells, Sol. Energy Mater. Sol. Cell. 159 (2017) 265–271.
[14] F. Feldmann, M. Nicolai, R. Müller, C. Reichel, M. Hermle, Optical and electrical characterization of poly-Si/SiOx contacts and their implications on solar cell design, Energy Procedia 124 (2017) 31–37.
[15] P. Padhamnath, A. Khanna, N. Nandakumar, N. Nampalli, V. Shanmugam, A. G. Aberle, S. Duttagupta, Development of thin polysilicon layers for application in monoPoly™ cells with screen-printed and fired metallization, Sol. Energy Mater. Sol. Cell. 207 (2020) 110358.
[16] Y. Chen, P.P. Altermatt, D. Chen, X. Zhang, G. Xu, Y. Yang, Y. Wang, Z. Feng, H. Shen, P.J. Verlinden, From laboratory to production: learning models of efficiency and manufacturing cost of industrial crystalline silicon and thin-film photovoltaic Technologies, IEEE Journal of Photovoltaics 8 (2018) 1531–1538.
[17] M.K. Stodolny, J. Anker, B.L.J. Geerligs, G.J.M. Janssen, B.W.H.v.d. Loo, J. Melskens, R. Santbergen, O. Isabella, J. Schmitz, M. Lenes, J.-M. Luchies, W.M. M. Kessels, I. Romijn, Material properties of LPCVD processed n-type polysilicon passivating contacts and its application in PERPoly industrial bifacial solar cells, SiliconPV 2017 (2017).
[18] S. Duttagupta, N. Nandakumar, P. Padhamnath, J.K. Buatis, R. Stangl, A.G. Aberle, monoPoly™ cells: large-area crystalline silicon solar cells with fire-through screen printed contact to doped polysilicon surfaces, Sol. Energy Mater. Sol. Cell. 187 (2018) 76–81.
[19] R.C.G. Naber, M. Lenes, A.H.G. Vlooswijk, J.R.M. Luchies, J. Wang, F. Zheng, J. Lin, Z. Zhang, n-PERT solar cells with passivated contact technology based on LPCVD polysilicon and fire-through contact metallization, Proc. of the 32nd European Photovoltaic Solar Energy Conference and Exhibition (2016) 430–433. München, Germany.
[20] Y. Chen, D. Chen, C. Liu, Z. Wang, Y. Zou, Y. He, Y. Wang, L. Yuan, J. Gong, W. Lin, X. Zhang, Y. Yang, H. Shen, Z. Feng, P.P. Altermatt, P.J. Verlinden, Mass production of industrial tunnel oxide passivated contacts (i-TOPCon) silicon solar cells with average efficiency over 23% and modules over 345 W, Prog. Photovoltaics Res. Appl. 27 (10) (2019) 827–834.
[21] F. Feldmann, T. Fellmeth, B. Steinhauser, H. Nagel, D. Ourinson, S. Mack, E. Lohmüller, J. Polzin, J. Benick, A. Richter, Large area TOPCon cells realized by a PECVD tube process, in: 36th European Photovoltaic Solar Energy Conference and Exhibition, 2019.
[22] D. Chen, Y. Chen, Z. Wang, J. Gong, C. Liu, Y. Zou, Y. He, Y. Wang, L. Yuan, W. Lin, R. Xia, L. Yin, X. Zhang, G. Xu, Y. Yang, H. Shen, Z. Feng, P.P. Altermatt, P. J. Verlinden, 24.58% total area efficiency of screen-printed, large area industrial silicon solar cells with the tunnel oxide passivated contacts (i-TOPCon) design, Sol. Energy Mater. Sol. Cell. 206 (2020) 110258.
[23] N. Nandakumar, J. Rodriguez, T. Kluge, T. Grosse, L. Fondop, N. Balaji, M. Konig, S. Duttagupta, Investigation of 23% monoPoly screen-printed silicon solar cells with an industrial rear passivated contact, in: IEEE 46th Photovoltaic Specialists Conference, PVSC), 2019, 2019.
[24] H. Kobayashi, K. Imamura, W.B. Kim, S.S. Im, Asuha, Nitric acid oxidation of Si (NAOS) method for low temperature fabrication of SiO2/Si and SiO2/SiC structures, Appl. Surf. Sci. 256 (2010) 5744–5756.
[25] D. Kane, R. Swanson, Measurement of the emitter saturation current by a contactless photoconductivity decay method, IEEE photovoltaic specialists conference 18 (1985) 578–583.
[26] P.P. Altermatt, H. Plagwitz, R. Bock, J. Schmidt, R. Brendel, M.J. Kerr, A. Cuevas, The surface recombination velocity at boron-doped emitters: comparison between various passivation techniques, in: Proceedings of the 21st European Photovoltaic Solar Energy Conference, WIP Renewable Energies Dresden, Germany, 2006, pp. 647–650.
[27] B. Hoex, J. Schmidt, R. Bock, P.P. Altermatt, M.C.M. van de Sanden, W.M. M. Kessels, Excellent passivation of highly doped p-type Si surfaces by the negative-charge-dielectric Al2O3, Appl. Phys. Lett. 91 (2007) 112107.
[28] C.W. Chen, M. Hermle, J. Benick, Y. Tao, Y.W. Ok, A. Upadhyaya, A.M. Tam, A. Rohatgi, Modeling the Potential of Screen Printed Front Junction CZ Silicon Solar Cell with Tunnel Oxide Passivated Back Contact, Progress in Photovoltaics: Research and Applications, 2016.